



A Triple-Band Terahertz Metamaterial Absorber Using Two Double Rectangular Patches Connected by Two Identical Gold Strips

Shengxiong Lai¹ · Haiquan Zhou^{2,3} · Liming Lu¹ · Zhuchuang Yang¹ · Wei Xu¹ · Huaxin Zhu¹ · Xiangyang Zhang¹ · Ben-Xin Wang¹

Received: 4 April 2022 / Accepted: 1 June 2022 / Published online: 22 June 2022
© The Minerals, Metals & Materials Society 2022

Abstract

In this paper, a triple-band terahertz metamaterial absorber composed of double rectangular patches connected by two identical gold strips is proposed and demonstrated. Simulation results show that the designed absorber can realize three discrete absorption peaks (labeled as A, B and C) with corresponding absorption rates of 99.21%, 91.75% and 96.12%. The physical mechanism of these absorption peaks is verified by the distribution of electric fields. Different numerical investigations on the proposed absorber are presented to explore the influence on the performance of the device. The application of the absorber in terms of the surrounding refractive index sensing is further discussed. It is found that the third resonance peak has an ultra-narrow line width of 0.0749 THz, sensitivity of 125 GHz/refractive index unit (RIU), quality factor (Q-factor) value of 32.7, and figure of merit of 1.66. These results mean that the suggested scheme has considerable applications in imaging, sensing, detecting and other terahertz-related regimes. The design can also be applied in other applications, such as silicon photovoltaics.

Keywords Terahertz metamaterials · near-perfect absorber · triple-band absorption · sensing

Introduction

The terahertz wave, which is located in the spectral frequency range from 0.1 THz to 10 THz, has attracted intense attention during the last few decades due to its unique characteristics,¹ such as excellent transmittance, wide bandwidth, and low photon energy.^{2,3} Meanwhile, because of its distinctive frequency domain location, the THz wave has features of microwave and infrared frequency bands, concurrently.⁴ However, the penetration of the THz wave enables it to pass through quite a number of natural materials, which greatly limits the development and application of terahertz technology. Until the emergence of metamaterials and their introduction into the terahertz region, the development of terahertz-related technologies has been gradually fruitful

in various fields, for instance, communications,^{5,6} sensing,⁷ imaging,⁸ molecule identification and nondestructive testing.^{9,10} Metamaterials are uniquely artificially designed electromagnetic composite materials with periodic subwavelength microarrays of metallic or dielectric materials. Using these materials achieves new remarkable properties that are not found in natural materials; researchers have developed many metamaterial devices that perform better than traditional optics, for example, filters, super lenses, absorbers, modulators and switches.^{11–14}

Metamaterial perfect absorbers have attracted extensive attention of researchers due to the advantages of perfect absorption, stealth technology, energy harvesting and sensitive sensing.^{15–50} A typical metamaterial perfect absorber is made up of three layers including a top layer of the periodic metal pattern, a middle layer of the insulator dielectric and a bottom layer of the metal substrate, respectively. Since the first metamaterial perfect absorber was put forward by Landy et al. in 2008,¹³ several metamaterial schemes have been proposed.^{19–23} Nevertheless, these absorbers are mostly single band, which has great limitations to the practical application of absorbers as they lack frequency selectivity and have poor sensitivity. In order to extend the application prospects and

✉ Ben-Xin Wang
wangbenxin@jiangnan.edu.cn

¹ School of Science, Jiangnan University, Wuxi 214122, China

² Zhejiang Beyondsun Green Energy Technology CO., LTD., Huzhou 313008, China

³ Zhejiang Beyondsun PV Co., Ltd., Huzhou 313008, China

potentials of metamaterial absorbers, multiple-band absorbers are urgently needed.

Generally, the strategies of the multiple-band can be realized through coplanar resonator arrangement or vertical stacking.^{24–31} For example, a quad-band metamaterial absorber with multiple layers of stacking in the vertical direction has been proposed by Wang et al. which stacks double layers of gold patch in the top space. They obtained absorption of more than 98% at four resonance frequency points.²⁴ A dual-band terahertz absorber was designed by Xing et al. which stacks graphene sheets and an array of graphene ribbon on the top.²⁵ This can adjust the resonance peaks by changing the chemical potentials of graphene. Although these stack-design methods can achieve multiple-band absorbers, it is inevitable to have the following shortcomings: difficult processing, complex structure, time-consuming structure optimization and difficult independent tuning. Therefore, researchers have mostly adopted the design scheme of ranking metallic patterns of different sizes within a coplanar unit lattice to reach multiple-band absorption.^{26–31} Pan et al. presented a dual-band metamaterial absorber based on a windmill-shaped surface structure.²⁶ Wang et al. demonstrated a triple-band metamaterial absorber employing a ring and four pairs of capacitor plates on the top space.²⁷ Sarkhel et al. designed a complex surface structure to realize ultrathin quad-band.²⁸ Furthermore, to gain five or even more absorption peaks, the number of sub-resonators will increase in the coplanar structure and the complexity of the device will significantly heighten.^{29,30} Thus, the study of metamaterial absorber using simple configuration and few resonators to achieve multiple-band perfect absorption in terahertz spectral region is still challenging.

In this paper, a simple triple-band metamaterial absorber design is presented. The suggested device comprises double rectangular patches connected by two identical gold strips. The triple-band near-perfect absorption is achieved at the terahertz region. The underlying physical mechanism of the triple-band absorption is discussed by means of the near-field distributions under each resonance peak. It is revealed that the combined effect of the localized resonance responses of the surface metallic structure gives rise to the multiple-band absorption. The influence of the geometric parameters of the unit-cell structure on the absorption properties of the proposed absorber is also studied. Results display that the first two absorption peaks exhibit a strong dependence on geometric parameters, and the third absorption peak can be independently regulated by period. Moreover, the sensing performance is explored based on the features of narrow band width and high-quality factor of the third absorption peak, and its comparison of sensing performance with previous works in Table I.

Table I Comparison of sensing performance between the proposed absorber and other absorbers operating in terahertz frequency region

FOM	Q	References
4.4	17.9	40
2.30	11.6	41
2.33	8.84	42
0.85	8.5	43
0.40	5.5	44
0.91	5.67	45
2.15	7.76	46
2.94	22.05	47
1.66	32.7	This paper

Structure Design and Model

Figure 1a shows the three-dimensional schematic diagram of the proposed triple-band terahertz metamaterial absorber, which consists of a metallic surface structure, a dielectric separation layer and a continuous metallic plane. The top view of the designed absorber is illustrated in Fig. 1b, the metallic pattern is made up of double rectangular patches connected by two identical gold strips. The double rectangular patches are the same size, of length $l_1 = 45 \mu\text{m}$ and width $l_2 = 30 \mu\text{m}$, and the distance between them equals the length of the horizontal gold strip ($l_3 = 20 \mu\text{m}$). The length of the horizontal gold strip is $w = 10 \mu\text{m}$, and the gap between the two identical gold strips is $d = 12 \mu\text{m}$. They are placed on dielectric metallic-based layers with a period of $P = 90 \mu\text{m}$. The middle dielectric separation layer can select polyimide (PI) as the insulating medium material, which has a dielectric constant of $3(1 + i0.06)$ and an optimized thickness of $t = 10 \mu\text{m}$.

The bottom continuous metallic plane and the surface structure are both made of Au, and the conductivity is $4.09 \times 10^7 \text{ S/m}$.^{18,24} The absorption of the absorber can be calculated by $A = 1 - T - R$, where A , T , and R are the coefficients of absorption, transmission, and reflection, respectively. Because the thickness of the bottom layer of the contiguous gold plane is greater than the skin depth of gold in the terahertz spectrum, the transmission (T) of the absorber is equal to zero.³² When the impedance of the metamaterial absorber matches that of the air by choosing an appropriate thickness of the dielectric layer, the reflection (R) can be also be made zero. The commercial simulation software FDTD Solutions is used to perform the proposed absorber. The plane terahertz wave is selected as the incident electromagnetic wave with the direction of incident parallel to the z -axis and perpendicular to the surface of the metamaterial absorber, and its electric field direction along the x -axis. In this simulation, the boundary conditions in the x and y directions are periodic and the perfectly matched layer is applied in the z direction.

Results and Discussion

The absorption characteristics of the suggested metamaterial absorber are shown in Fig. 2a. As observed, three discrete resonance peaks (marked as A, B and C) are located at 0.84 THz, 2.55 THz and 3.27 THz with the corresponding absorptivity of 99.2%, 91.7% and 96.1%, respectively. In order to more objectively illustrate the performance of absorption peaks, the full width at half maximum (FWHM) is calculated as 0.170 THz, 0.259 THz and 0.075 THz, respectively. The FWHM is an important performance indicator of the metamaterial device. We noted that peak A and peak B are perfect absorption peaks in the conventional sense, but absorption peak C has a quite narrow line width which has significant application prospects in terahertz sensing and detecting.^{17,26} Additionally, because the surface metallic pattern is asymmetrical, the performance of the triple-band absorber possesses a strong dependence on the polarization angle of incident light, see Fig. 2b.

To investigate the physical mechanism of the resonance peaks, the near-field distributions of the suggested triple-band absorber is provided. Figure 3a, b and c are, respectively, the electric field ($|E|$) distributions of the resonance frequency at peak A, peak B and peak C. The electric field (E_z) distributions of the corresponding absorption peaks are exhibited in Fig. 3d, e and f. Figure 3g–i and Fig. 3j–l, respectively, give the magnetic field ($|H_y|$) distributions of the insulating medium layer under the surface structure along the upper and lower dotted lines, as given in Fig. 3a–c.

For absorption peak A at 0.84 THz, its electric fields ($|E|$ and E_z) in Fig. 3a and d have similar distribution features that are mainly concentrated on both edges of the rectangular metal patches, while pretty weak field distributions are found at other lattice positions. The results indicate that

resonance peak A should originate from the fundamental mode localized resonance response of the whole top metallic pattern. The surface metallic pattern interacts with the incident beam, which generates the dipole resonance that interacts with the bottom gold plate to generate anti-parallel current, so the induced magnetic fields are focused on the middle insulator dielectric layer under the surface structure. The magnetic field ($|H_y|$) distribution shown in Fig. 3g indeed fits this analysis, as its field is strongly distributed at the insulator dielectric layer under the middle area of the whole surface structure. However, the magnetic field ($|H_y|$) distribution along the lower dotted line presented in Fig. 3j has some differences because the rectangular air gap does not generate a parallel current, which leads to weakened magnetic field ($|H_y|$) aggregation of the middle dielectric layer close to the air gap.

The electric field ($|E|$ and real E_z) distributions of the absorption peak B at 2.55 THz are given in Fig. 3b and e. It is clearly observed that the electric field ($|E|$) is discontinuously scattered around the edges of rectangular patches, and the electric field E_z is strongly scattered at the region approaching the connection of strips. Moreover, we especially noticed that the resonant frequency of peak B is more than three times that of the resonant frequency of peak A. These analyses illustrate that absorption peak B should be mainly derived from the fundamental mode localized resonance response of the strips because the length of the strips (l_3) is less than one third of the whole top metallic pattern. Meanwhile, the magnetic field ($|H_y|$) distribution is also gathered only in the middle dielectric layer under the connection strips due to the clustering of strong electric fields (E_z) caused by its fundamental mode resonance, as demonstrated in Fig. 3h and k. Similarly, the rectangular air gap can also have an impact on the magnetic field ($|H_y|$) distribution (Fig. 3k).

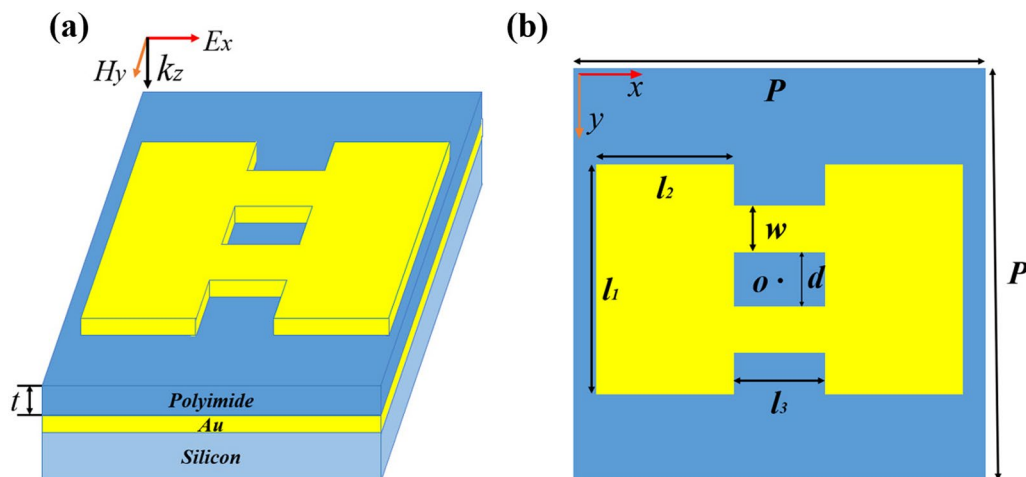


Fig. 1 (a) Three-dimensional schematic diagram of the unit cell of the multi-band terahertz metamaterial absorber; (b) Top view of schematic diagram of the unit cell of the multi-band terahertz metamaterial absorber.

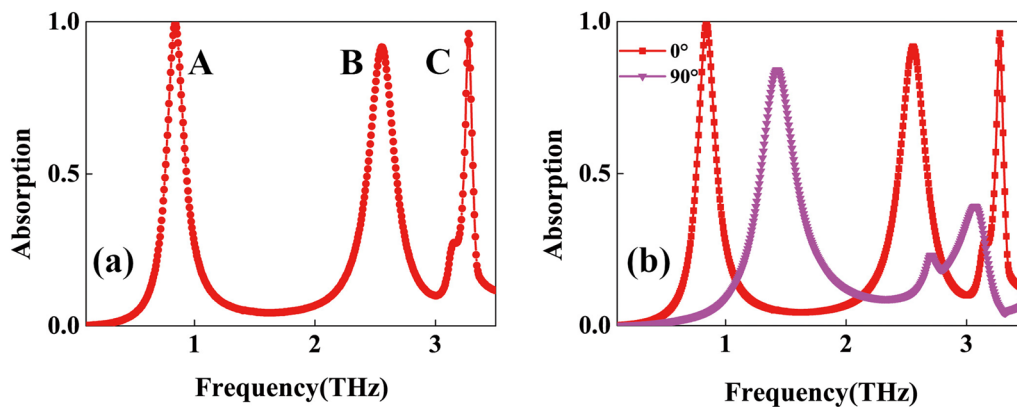


Fig. 2 (a) Simulated absorption curve of quad-band metamaterial absorber; (b) dependence of the absorption spectrum on the changes of polarization angle.

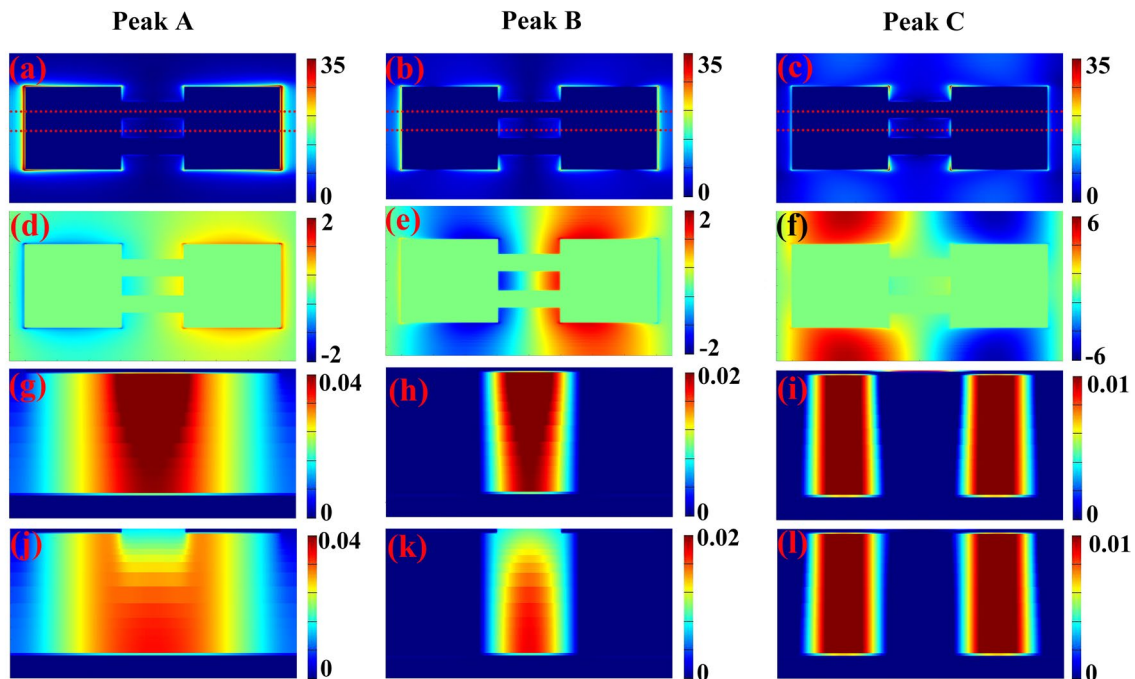


Fig. 3 Distribution of the electric field ($|E|$): (a) mode A, (b) mode B, (c) mode C; distribution of the electric field's z component (E_z): (d) mode A, (e) mode B, (f) mode C; distribution of the magnetic field's y component ($|H_y|$) in the middle dielectric layer along the upper dotted

lines: (g) mode A, (h) mode B, (i) mode C; distribution of the magnetic field's y component ($|H_y|$) in the middle dielectric layer along the lower dotted lines: (j) mode A, (k) mode B, (l) mode C.

Different from the cases of absorption peaks A and B, the electric field ($|E|$) of absorption peak C is chiefly accumulated at the corner of the middle notch position, and its electric field (E_z) is not only distributed over the upper and lower edges of the rectangular patches but also centered on the non-metallic areas, while the field distributions of the connection strips and rectangular air gap

are negligible. Thus, we preliminarily consider that the physical mechanism of absorption peak C results from the localized resonances and lattice resonances of the rectangular patches. The magnetic field ($|H_y|$) distribution in Fig. 3i and h exactly tally with this prediction, the strong field aggregation can only be observed in the insulator dielectric layer under the rectangular patches.

In order to further investigate and evaluate the resonance properties of the triple-band absorption device, the variation of geometric parameters of the structure is discussed. In view of the aforementioned theoretical explanations of the near-field distribution of the proposed triple-band absorber, we first consider the influence of the dimension of the rectangular patch, i.e., the length of l_1 and the width of l_2 . It is known that the frequency of the localized resonance response of the metallic arrays is in reverse proportion to their length; therefore, small frequencies correspond to large lengths of the localized resonance response. This may also explain why absorption peak A results from the fundamental mode resonance response. As observed in Fig. 4a and b, the size variations of the rectangular patch can affect the resonance frequency of absorption peaks A and B whereas they have slight effects for the resonance frequency of absorption peak C. Similar frequency shift features are also discovered in Fig. 4c and d. In addition, it is worth noting that there is barely an effect on the three resonance frequencies when the rectangular air gap width (d) varies, since the connection strips were simply moved without a change in dimension (see Fig. 4e). However, the physical origin of absorption peak C is different from that of absorption peaks A and B because the formation of its physical mechanism is chiefly derived from the surface lattice resonance. Predictably, the dependence of absorption peak C on the period is very strong. Figure 4f also testified that absorption peak C is extraordinarily sensitive to changes of the period and hardly affect absorption peaks A and B.^{33–35}

On account of the narrow band width of absorption peak C, we next study the response of the designed absorber to the refractive index (n) variation of the surrounding. As

illustrated in Fig. 5a, we covered the surface of the device with a layer of analyte with a thickness of $s = 2 \mu\text{m}$. It is obvious that resonance peak A barely shifts, while resonance peaks B and C are fully sensitive to the surrounding as the refractive index (n) of the analysis changes from 1.0 to 1.8 (step 0.2). The relationship between the three resonance frequency points and the variations of the refractive index is supplied in Fig. 5b. Sensing sensitivity (S) is a significant factor used to estimate the sensing performance; it is defined as^{36–39} $S = \Delta f / \Delta n$, where Δf and Δn are, respectively, the changes of the resonance frequency and refractive index. Herein, the sensitivity (S) is 188 GHz/RIU (refractive index unit) for resonance peak B and 125 GHz/RIU for resonance peak C. In fact, the FOM (figure of merit) is usually calculated to characterize the sensing performance of the device. FOM is defined as^{36–39} $\text{FOM} = \Delta f / (\Delta n \times \text{FWHM})$. Combined with the calculation data in Fig. 5a and b, the FOM of peak B is 0.72 and peak C is 1.66. Furthermore, the quality factor (Q) is another intuitive indicator in assessing the sensing performance of the resonance mode; it is defined as^{36–39} $Q = f_0 / \text{FWHM}$, where f_0 is the central resonance frequency. According to the definition of the Q value, the value of resonance peak C is up to 32.7, which is larger than that of resonance peak B with a Q of 17. Meanwhile, the sensing performance of the designed device surpasses many reported metamaterial absorbers, see below, Table I. The high- Q value of resonance peak C has potential applications in terahertz sensing.

The different thickness (s) of the analyte layer will also impact the absorption spectra, see Fig. 5c. The result hints that the resonance peak C has a distinct redshift when s increases from 2 to $14 \mu\text{m}$ with a step of $6 \mu\text{m}$, while the

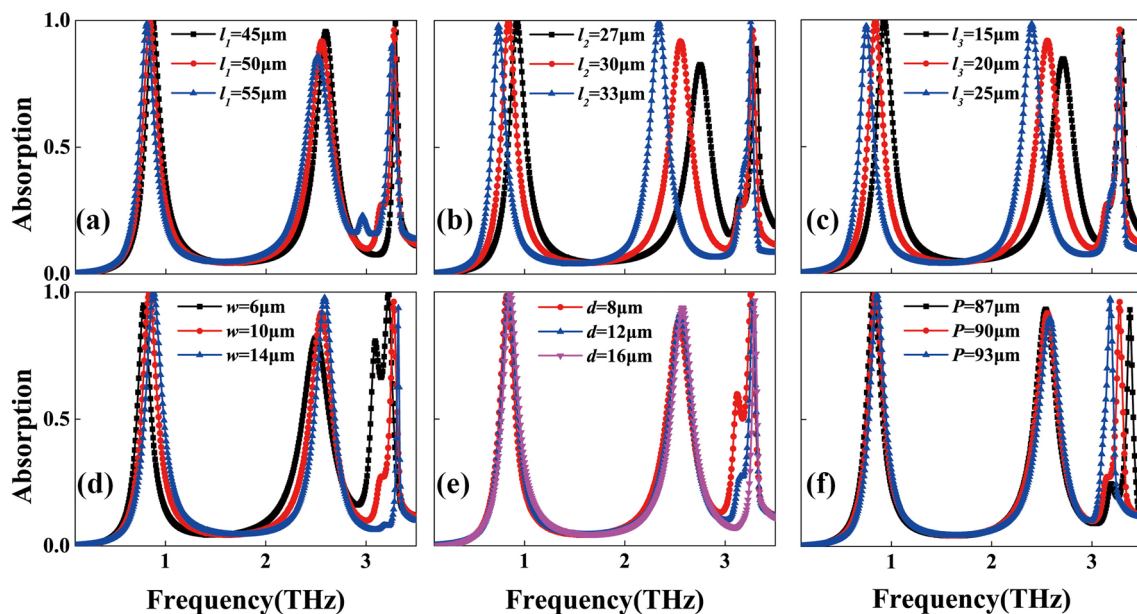


Fig. 4 Influences of structural parameters l_1 (a), l_2 (b), l_3 (c), w (d), d (e), and P (f) on the absorption spectra.

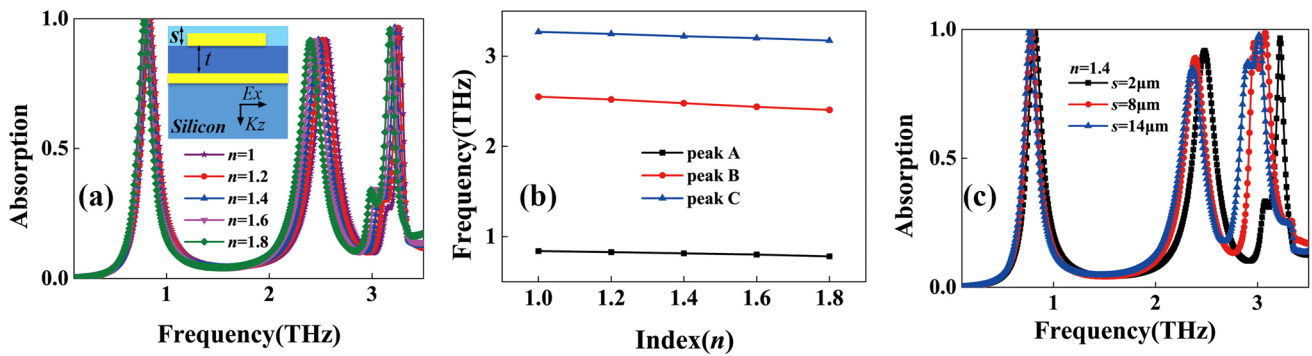


Fig. 5 (a) The absorption spectra of the analytes with different refractive indices (n); (b) relationship between the three resonance peaks and the refractive indices (n) of the analytes; (c) absorption spectra of the analytes with different thickness s .

frequency shift of resonance peak B is weaker than that of resonance peak C and its absorption rate also decreased. In general, the analyte with different thickness will affect the effective refractive index of the device, resulting in the shift of the frequency point. To sum up, absorption peak C is more advantageous than absorption peak B in distinguishing the unknown analytes.

Conclusions

In summary, a multiple-band terahertz metamaterial absorber based on a simple configuration (double rectangular patches connected by two identical gold strips) is reported. Numerical simulation results show that the designed structure achieves a triple-band near-perfect absorption with corresponding absorbance of 99.2%, 91.7% and 96.1%, respectively. Analysis of their near-field distribution explains the physical origin of the suggested scheme. The first two absorption peaks mainly come from the fundamental mode response of the surface metallic pattern, and thus exhibit a strong dependence on geometric parameters. The third absorption peak is chiefly formed at the combined effect of the localized resonance response of the surface metallic pattern and the surface lattice resonance of the device, so it can be independently regulated by period. Additionally, the sensing performance of the proposed absorber has been assessed by covering the top layer with an analyte. As a consequence, the third absorption peak responds sensitively to changes in the refractive index of the surroundings, and its sensing sensitivity, figure of merit, and quality factor are 125 GHz/RIU, 1.66, 32.7, respectively. The designed triple-band metamaterial absorber has promising potential in terahertz sensing, imaging and detecting.

Author Contributions S.L. created the models, did the simulation, discussed the results, analyzed the data, wrote the original manuscript.

H.Z. created the models, did the simulation, discussed the results, discussed the results. L.L. discussed the results, analyzed the data, revised the manuscript. Z.Y. did the simulation, discussed the results, analyzed the data. W.X. did the simulation, discussed the results. H.Z. discussed the results, analyzed the data. X.Z. discussed the results, analyzed the data. B.X.W. supervised this project, provided the original idea and funding, discussed the results, analyzed the data, revised the manuscript.

Funding This research was funded by National Natural Science Foundation of China (62105128), and Innovation Team Project of Zhejiang Province (2019R01012).

Data Availability The data and material that support the findings of this study are available from the corresponding author upon reasonable request.

Conflict of interest The authors declare no competing interests.

Consent to Participate All authors in this article have agreed to participate in the publication of this article.

Consent for publication We, the co-authors, give consent for information about the manuscript to be published.

Ethics Approval Not Applicable.

References

1. G.P. Williams, Filling the THz gap—High Power Sources and Applications. *Rep. Prog. Phys.* 69, 301 (2005).
2. M. Shalaby, C. Vicario, and C.P. Hauri, High-Performing Non-linear Visualization of Terahertz Radiation on A Silicon Charge-Coupled Device. *Nat. Commun.* 6, 8439 (2015).
3. J. Kang and Q. Park, Local Enhancement of Terahertz Waves in Structured Metals. *IEEE Transa. Terahertz Sci. Technol.* 6, 371 (2016).
4. J. Yang, Z. Zhu, J. Zhang, C. Guo, W. Xu, K. Liu, X. Yuan, and S. Qin, Broadband Terahertz Absorber based on Multi-band Continuous Plasmon Resonances in Geometrically Gradient Dielectric-Loaded Graphene Plasmon Structure. *Sci. Rep.* 8, 3239 (2018).

5. J.M. Jornet and I.F. Akyildiz, Graphene-Based Plasmonic Nano-Antenna for Terahertz Band Communication in Nanonetworks. *IEEE J. Sel. Areas Commun.* 31, 685 (2013).
6. A. Singh, M. Andreello, N. Thawdar, and J.M. Jornet, Design and Operation of A Graphene-Based Plasmonic Nano-Antenna Array for Communication in the Terahertz Band. *IEEE J. Sel. Areas Commun.* 38, 2104 (2020).
7. F. Zangeneh-Nejad and R. Safian, A Graphene-Based thz Ring Resonator for Label-Free Sensing. *IEEE Sens. J.* 16, 4338 (2016).
8. X. Yang, X. Zhao, K. Yang, Y. Liu, Y. Liu, W. Fu, and Y. Luo, Biomedical Applications of Terahertz Spectroscopy and Imaging. *Trends Biotechnol.* 34, 810 (2016).
9. J. Huang, J. Liu, K. Wang, Z. Yang, and X. Liu, Classification and Identification of Molecules Through Factor Analysis Method Based on Terahertz Spectroscopy. *Spectrochim. Acta Part A Mol. Biomol. Spectrosc.* 198, 198 (2018).
10. K. Peng, P. Parkinson, J.L. Boland, Q. Gao, Y.C. Wenas, C.L. Davies, Z. Li, L. Fu, M.B. Johnston, H.H. Tan, and C. Jagadish, Broadband Phase-Sensitive Single Inp Nanowire Photoconductive Terahertz Detectors. *Nano Lett.* 16, 4925 (2016).
11. P. Pitchappa, A. Kumar, R. Singh, and N. Wang, Electromechanically Tunable Frequency-Agile Metamaterial Bandpass Filters for Terahertz Waves. *Adv Optical Mater.* 10, 2101544 (2022).
12. X. Zhang and Z. Liu, Superlenses to Overcome the Diffraction Limit. *Nat. Mater.* 7, 435 (2008).
13. N.I. Landy, S. Sajuyigbe, J.J. Mock, D.R. Smith, and W.J. Padilla, Perfect Metamaterial Absorber. *Phys. Rev. Lett.* 100, 207402 (2008).
14. X. Zhang and Y.-S. Lin, Actively Electromagnetic Modulation of IHI-Shaped Terahertz Metamaterial with High-efficiency Switching Characteristic. *Result Phys.* 15, 102532 (2019).
15. J. Kim, K. Han, and J.W. Hahn, Selective Dual-Band Metamaterial Perfect Absorber for Infrared Stealth Technology. *Sci. Rep.* 7, 6740 (2017).
16. T.S. Almomneef and O.M. Ramahi, Metamaterial Electromagnetic Energy Harvester with Near Unity Efficiency. *Appl. Phys. Lett.* 106, 153902 (2015).
17. D. Hu, T. Meng, H. Wang, Y. Ma, and Q. Zhu, Ultra-Narrow-Band Terahertz Perfect Metamaterial Absorber for Refractive Index Sensing Application. *Results Phys* 19, 103567 (2020).
18. B.-X. Wang, Y. He, P. Lou, and W. Xing, Design of A Dual-Band Terahertz Metamaterial Absorber Using Two Identical Square Patches for Sensing Application. *Nanoscale Adv.* 2, 763 (2020).
19. X. Liu, T. Starr, A.F. Starr, and W.J. Padilla, Infrared Spatial and Frequency Selective Metamaterial with Near-Unity Absorbance. *Phys. Rev. Lett.* 104, 207403 (2010).
20. Y. Cheng, H. Yang, Z. Cheng, and N. Wu, Perfect Metamaterial Absorber Based on a Split-Ring-Cross Resonator. *Appl. Phys. A* 102, 99 (2011).
21. J. Grant, Y. Ma, S. Saha, L.B. Lok, A. Khalid, and D.R.S. Cumming, Polarization Insensitive Terahertz Metamaterial Absorber. *Opt. Lett.* 36, 1524 (2011).
22. Q. Shen and H. Xiong, An Amplitude and Frequency Tunable Terahertz Absorber. *Results Phys.* 34, 105263 (2022).
23. Z. Wang, Y. Ou, S. Wang, Y. Meng, Z. Wang, X. Zhai, L. Wang, and S. Xia, Ultrahigh-Q Tunable Terahertz Absorber Based on Bulk Dirac Semimetal with Surface Lattice Resonance. *Photonics* 9, 22 (2022).
24. B.-X. Wang, Q. Xie, G. Dong, and W.-Q. Huang, Quad-Spectral Perfect Metamaterial Absorber at Terahertz Frequency Based on a Double-Layer Stacked Resonance Structure. *J. Electron. Mater.* 48, 2209 (2019).
25. R. Xing and S. Jian, A dual-Band Thz Absorber Based on Graphene Sheet and Ribbons. *Opt. Laser Technol.* 100, 129 (2018).
26. W. Pan, T. Shen, Y. Ma, Z. Zhang, H. Yang, X. Wang, X. Zhang, Y. Li, and L. Yang, Dual-Band and Polarization-Independent Metamaterial Terahertz Narrowband Absorber. *Appl. Opt.* 60, 2235 (2021).
27. Y. Wang, Z. Chen, D. Xu, Z. Yi, X. Chen, J. Chen, Y. Tang, P. Wu, G. Li, and Y. Yi, Triple-Band Perfect Metamaterial Absorber with Good Operating Angle Polarization Tolerance Based on Split Ring Arrays. *Results Phys.* 16, 102951 (2020).
28. A. Sarkhel and S.R.B. Chaudhuri, Compact Quad-Band Polarization-Insensitive Ultrathin Metamaterial Absorber with Wide Angle Stability. *IEEE Antennas Wirel. Propag. Lett.* 16, 3240 (2017).
29. Y. He, Q. Wu, and S. Yan, Multi-Band Terahertz Absorber at 0.1–1 THz Frequency Based on Ultra-Thin Metamaterial. *Plasmonics* 14, 1303 (2019).
30. W. Jia, J. Bai, K. Roberts, K.Q. Le, and D. Zhou, Design and Simulation of A Polarization-Insensitive Metamaterial Terahertz Absorber with Five Bands. *Microw. Opt. Technol. Lett.* 62, 2649 (2020).
31. JGe.Y.H. ZhangDong, and L. Zhang, Nanolayered VO₂-Based Switchable Terahertz Metasurfaces as Near-Perfect Absorbers and Antireflection Coatings. *ACS Appl. Nano Mater.* 5, 5569 (2022).
32. G.-D. Liu, X. Zhai, H.-Y. Meng, Q. Lin, Y. Huang, C.-J. Zhao, and L.-L. Wang, Dirac Semimetals Based Tunable Narrowband Absorber at Terahertz Frequencies. *Opt. Express* 26, 11471 (2018).
33. Z. Li, S. Butun and K. Aydin, Ultranarrow Band Absorbers Based on Surface Lattice Resonances in Nanostructured Metal Surfaces. *ACS Nano* 8, 8242 (2014).
34. M. Manjappa, Y.K. Srivastava, and R. Singh, Lattice-Induced Transparency in Planar Metamaterials. *Phys. Rev. B* 94, 161103 (2016).
35. V.G. Kravets, A.V. Kabashin, W.L. Barnes, and A.N. Grigorenko, Plasmonic Surface Lattice Resonances: A Review of Properties and Applications. *Chem. Rev.* 118, 5912 (2018).
36. J.N. Anker, W.P. Hall, O. Lyandres, N.C. Shah, J. Zhao, and R.P. Van Duyne, Biosensing with Plasmonic Nanosensors. *Nat. Mater.* 7, 442 (2008).
37. X. Hu, G. Xu, L. Wen, H. Wang, Y. Zhao, Y. Zhang, D.R.S. Cumming, and Q. Chen, Metamaterial Absorber Integrated Microfluidic Terahertz Sensors. *Laser Photon. Rev.* 10, 962 (2016).
38. R. Yahiaoui, S. Tan, L. Cong, R. Singh, F. Yan, and W. Zhang, Multispectral Terahertz Sensing with Highly Flexible Ultrathin Metamaterial Absorber. *J. Appl. Phys.* 118, 083103 (2015).
39. X. Yu, L. Shi, D. Han, J. Zi, and P.V. Braun, High Quality Factor Metalodielectric Hybrid Plasmonic–Photonic Crystals. *Adv. Func. Mater.* 20, 1910 (2010).
40. K.Q. Le, Q.M. Ngo, and T.K. Nguyen, Nanostructured Metal–Insulator–Metal Metamaterials for Refractive Index Biosensing Applications: Design, Fabrication, and Characterization. *IEEE J. Sel. Top. Quantum Electron.* 23, 388 (2017).
41. L. Cong, S. Tan, R. Yahiaoui, F. Yan, W. Zhang, and R. Singh, Experimental Demonstration Of Ultrasensitive Sensing With Terahertz Metamaterial Absorbers: A Comparison with the Metasurfaces. *Appl. Phys. Lett.* 106, 031107 (2015).
42. N. Liu, M. Mesch, T. Weiss, M. Hentschel, and H. Giessen, Infrared Perfect Absorber and its Application as Plasmonic Sensor. *Nano Lett.* 10, 2342 (2010).
43. Y. Li, X. Chen, F. Hu, D. Li, H. Teng, Q. Rong, W. Zhang, J. Han, and H. Liang, Four Resonators Based High Sensitive Terahertz Metamaterial Biosensor Used for Measuring Concentration of Protein. *J. Phys. D Appl. Phys.* 52, 095105 (2019).
44. R. Cheng, L. Xu, X. Yu, L. Zou, Y. Shen, and X. Deng, High-Sensitivity Biosensor for Identification of Protein Based on Terahertz Fano Resonance Metasurfaces. *Opt. Commun.* 473, 125850 (2020).
45. F. Shen, J. Qin, and Z. Han, Planar Antenna Array as a Highly Sensitive Terahertz Sensor. *Appl. Opt.* 58, 540 (2019).

46. F. Cheng, X. Yang, and J. Gao, Enhancing Intensity and Refractive Index Sensing Capability with Infrared Plasmonic Perfect Absorbers. *Opt. Lett.* 39, 3185 (2014).
47. A.S. Saadeldin, M.F.O. Hameed, E.M.A. Elkaramany, and S.S.A. Obayya, Highly Sensitive Terahertz Metamaterial Sensor. *IEEE Sens. J.* 19, 7993 (2019).
48. B.-X. Wang, C. Xu, G. Duan, J. Jiang, W. Xu, Z. Yang, and Y. Wu, Miniaturized and Actively Tunable Triple-Band Terahertz Metamaterial Absorber Using an Analogy I-Typed Resonator. *Nanoscale Res. Lett.* 17, 35 (2022).
49. B.X. Wang, Y. He, P. Lou, and H. Zhu, Multi-Band Terahertz Superabsorbers Based on Perforated Square-Patch Metamaterials. *Nanoscale Adv.* 3, 455 (2021).
50. B.X. Wang, W. Xu, Y. Wu, Z. Yang, S. Lai, and L. Lu, Realization of a Multi-Band Terahertz Metamaterial Absorber Using Two Identical Split Rings Having Opposite Opening Directions Connected by a Rectangular Patch. *Nanoscale Adv.* 4, 1359 (2022).

Publisher's Note Springer Nature remains neutral with regard to jurisdictional claims in published maps and institutional affiliations.